Highly-mismatched InAs/InSe heterojunction diodes

A. V. Velichko[1*], Z. R. Kudrynskyi[1], D. M. Di Paola[1], O. Makarovskiy[1],

M. Kesaria[2], A. Krier[2], I. C. Sandall[3,4], C. H. Tan[3], Z.D. Kovalyuk[5], A. Patanè[1*]

[1]*School of Physics and Astronomy, the University of Nottingham, Nottingham NG7 2RD, UK*

[2]*Physics Department, Lancaster University, Lancaster LA1 4YB, UK*

[3]*Department of Electronic & Electrical Engineering, the University of Sheffield, Sheffield S1 3JD, UK*

[4]*Department of Electrical Engineering and Electronics, the University of Liverpool, Liverpool, L69 3GJ, UK*

[5]*Frantsevich Institute for Problems of Materials Science, The National Academy of Sciences of Ukraine, Chernivtsi Branch, Chernivtsi 58001, Ukraine*

Abstract

We report on heterojunction diodes prepared by exfoliation and direct mechanical transfer of a *p*-type InSe thin film onto an *n*-type InAs epilayer. We show that despite the different crystal structures and large lattice mismatch (~34%) of the component layers, the junctions exhibit rectification behaviour with rectification ratios of ~10^4 at room temperature and broad-band photoresponse in the near infrared and visible spectral ranges.

*Corresponding authors:

amalia.patane@nottingham.ac.uk

a.velychko@nottingham.ac.uk

School of Physics and Astronomy, the University of Nottingham, Nottingham NG7 2RD, UK

Phone: +44 115 9515185

Heterostructures made by mechanical exfoliation and vertical stacking of van der Waals (vdW) crystals are being intensively studied (see [1-3] and references therein). Because the component layers are held together by weak van der Waals forces, both the structural integrity and the electronic properties of the individual atomic sheets are preserved, thus enabling high-quality interfaces and devices [1]. On the other hand, heterostructures that combine vdW crystals with traditional semiconductors, such as GaAs, InAs, Ge have received less attention [4-6]. Of particular interest are *p*-*n* diodes that combine a vdW crystal with a narrow bandgap semiconductor, such as InAs (band gap energy E_g = 0.35 eV at 300 K). The optical response of the component layers of the diode over distinct spectral ranges could offer a plethora of strategically important near-infrared (NIR) and mid-infrared (MIR) optoelectronic applications, including remote gas sensing, health and security [7].

In this Letter, we report on heterojunction diodes prepared by exfoliation and direct mechanical transfer of a *p*-type InSe thin film onto an *n*-type InAs epilayer (see Figure 1a). The InSe compound is a vdW semiconductor with electronic properties that are unprecedented within the wide family of vdW crystals. Its high electron mobility (up to 10^3 $cm^2V^{-1}s^{-1}$ at 300 K) [8], *p*- or *n*-type doping [9], tunable band gap from the NIR (E_g = 1.26 eV at 300K) to the visible (VIS) range [10], as well as chemical stability in air [11], represent attractive features for versatile band engineering and reliable devices for electronics and optoelectronics. Recent reports have demonstrated optical devices based on heterostructure stacks of InSe and other vdW crystals (*e.g.* GaSe, graphene, and $CuInSe_2$) [9, 12-13] or oxides (*e.g.* CdO, and ZnO) [14-15], and *p*-*n* junctions based on surface functionalization of *n*-InSe [16]. Here we report on a heterojunction that combines the NIR *p*-InSe with the MIR *n*-InAs. We show that despite the different crystal structures and large lattice mismatch (~34%) of the component layers, the junction exhibits diode-like behaviour

with rectification ratios of ~10^4 and broad-band photoresponse in the NIR and VIS spectral ranges, with the potential to be extended to the MIR region.

Our γ-polytype *p*-type InSe crystals were grown by the Bridgman method from a polycrystalline melt of $In_{1.03}Se_{0.97}$ using Cd as the *p*-type dopant. The primitive unit cell of γ-InSe is shown in Figure 1a: it consists of three layers, each comprising four covalently bonded monoatomic sheets in the sequence Se-In-In-Se; along the *c*-axis, the lattice constant is c = 24.961 Å and, within each *a*-*b* plane, atoms form hexagons with lattice parameter a_{InSe} = 4.002 Å [10]. The van der Waals gap between adjacent layers is of 0.38 nm. The Hall concentration of holes in *p*-InSe is $n_p = 6x10^{20}$ m^{-3} at room temperature (T = 300 K) and decreases significantly with lowering T below 200K due to freezing of carriers onto the Cd-acceptor levels. The InAs epilayer (thickness d=1.0 μm) was grown by Molecular Beam Epitaxy (MBE) on a semi-insulating (100)-oriented GaAs substrate, which provides effective isolation for electrical measurements. The nominally undoped InAs epilayer has *n*-type conductivity with a Hall concentration of electrons $n_e = 8.8x10^{21}$ m^{-3} at T = 300 K, which is weakly dependent on T down to 2 K. Following oxygen plasma cleaning of the *n*-InAs surface, a thin film of *p*-InSe was mechanically exfoliated from as-grown crystals with adhesive tape and transferred onto the *n*-InAs layer. The *p*-InSe flakes have thickness in the range t = 1-10 μm and in-plane area A = 2-5 mm^2. Metal contacts were made to InAs with indium and to the top *p*-InSe layer with silver paste. In the following, we define positive bias with the *p*-InSe layer biased positively.

The in-plane lattice mismatch between InSe and InAs is $(a_{InAs}-a_{InSe})/a_{InAs}$ ~ 34%, where a_{InAs} = 6.058 Å and a_{InSe} = 4.002 Å are the in-plane lattice constants of InAs and InSe, respectively. Despite this large lattice mismatch, the current-voltage (*I*-*V*) characteristics of the heterojunctions show diode-like behavior at T = 300 K, see Figure 1b. The *I*-*V*s reveal a number of common

features: a low leakage current density (J < 10 mA/cm^2) in reverse bias that is weakly dependent on V up to V ~ -4 V; and an exponential increase of the current, which becomes steeper around a "knee" at V ~ 1 V (see inset of Figure 1b). The analysis of the I-V characteristics of these devices using the Shockley equation give ideality factors (η > 2) that are larger than those expected for conventional p-n diodes (η = 1-2) and those reported for InAs/WSe_2 [4]. These larger ideality factors can be caused by low carrier mobilities and carrier localization, which are not considered in the Shockley equation [17]. We have conducted Hall-mobility studies of both n-type InAs and p-type InSe. The room temperature Hall mobility of holes in p-type InSe is μ_h ~ 10 cm^2/Vs, significantly smaller than that of electrons in n-type InAs (μ_e ~ 10^4 cm^2/Vs).

We note that the diode-like behavior is stable and reproducible over multiple runs; the stability relies on the formation of a good mechanical contact between the n-InAs and p-InSe layers. This requires the use of layers with clean surfaces: the InAs epilayer was cleaned in oxygen plasma that was found to increase the rectification ratios by more than an order of magnitude. The InSe flakes were not cleaned after the exfoliation as they are stable in air [11], they have a smooth surface with a low-density of surface states, and a well-defined thickness [9].

For the measurements of the photocurrent, ΔI, light from a 250 W quartz halogen lamp was dispersed through a 0.25 m monochromator and modulated with a mechanical chopper (at a frequency f = 187 Hz); a Stanford SR830 lock-in amplifier was used to measure the voltage drop ΔV_R across a series load resistor (R = 1kΩ) from which we derived $\Delta I = \Delta V_R/R$. Figure 2 shows the spectral dependence of ΔI at V = 0 for two representative heterojunctions: we observe a broad-band photoresponse from the NIR to the VIS range with a peak at a photon energy hv = 1.25 eV, which corresponds to the excitonic absorption of bulk InSe [10]. The photocurrent spectra also reveal regular interference fringes with periodicity ΔE. The interference condition for a maximum in the

interference pattern and light propagating in the direction perpendicular to the layers (see the inset in Figure 2) is given by $E_m = mhc/2nt$, where t is the flake thickness, n = 2.7 is the refractive index of InSe [18], h is the Planck constant, e is the electron charge, m is the order of interference, and E_m is the photon energy corresponding to the m^{th}-order.

From the periodicity $\Delta E = hc/2nt$ of the interference pattern, we estimate the thickness of the InSe flake, which is t = 3.5 and 5.7 μm for the two heterojunctions shown in Figure 2. Further inspection of the spectra reveals that the two junctions have a slightly different spectral response. As the thickness of the InSe flake increases, the photocurrent becomes smaller at high photon energies. For thick InSe layers, the high energy incident photons are mostly absorbed near the surface of InSe where they recombine before reaching the depletion region of the junction.

In reverse bias the photocurrent increases with increasing intensity of the incident light (Figure 3a) or with increasing applied voltage (Figure 3b). From the power P of light incident at the interface of the junction and the exponential attenuation of light across an InSe flake of thickness t = 5.7 μm, we estimate the photoresponsivity, $R = \Delta I/[P \times exp(-\alpha t)]$. For V = 0V and α = 5.2×10^5 m^{-1} (1.0×10^5 m^{-1}) at λ = 633 nm (984 nm) [19], we find values for R of up to 0.2 A/W (0.02 A/W) at λ = 633 nm (984 nm) and $P \sim 10^{-7}$ W (see Figure 3c). A photoresponse was also observed at MIR wavelengths (λ = 2000 nm), but with responsivity ($< 10^{-4}$ A/W) significantly smaller than that in the NIR.

For positive applied voltages, the contribution of the photocurrent to the total current is relatively small compared to that for negative biases. For example, for V = -1V, the current can increase by nearly 2 orders of magnitude for P = 6 μW, whereas at the corresponding positive bias V = +1V, the change in the current is much smaller (see Figure 3a). Also, we note that around the 'knee' in I-V, the change in the current is more significant. As shown in the inset of Figure 3a,

under light illumination the current decreases relative to the dark value for $V < 1.8$V and increases for $V > 1.8$V.

To explain our findings, we model the energy band diagram of the junction by solving the Poisson's equation (Figure 4). Since the band alignment at the InAs/InSe heterostructure interface is not known, to estimate the height of the potential steps (ΔE_C and ΔE_V) of the conduction band (CB) and valence band (VB) edges at the heterostructure interface, we use the electron affinity (χ) and band gap energy (E_g) of InAs ($\chi = 4.9$ eV, $E_g = 0.35$ eV) and InSe ($\chi = 4.6$ eV, $E_g = 1.26$ eV). This gives $\Delta E_C = 0.30$ eV and $\Delta E_V = 0.61$ eV (Figure 4a). Furthermore, from the concentration of dopants in the *n*-InAs and *p*-InSe layers [20], we calculate the built-in potential $\phi_B = 0.58$ V at $V = 0$V and the corresponding depletion region width $W = W_n + W_p = 694$ nm, where $W_n = 44$ nm and $W_p = 650$ nm are the depletion widths in the *n*- and *p*-type layers, respectively [21].

The energy band profiles from this simple model explain the rectification behavior of the junction: The built-in potential increases for $V < 0$ (Figure 4b) and decreases for $V > 0$ (Figure 4c), thus leading to a corresponding decrease and increase of the current, respectively. To explain the steep increase of the dark current at $V \sim 1$ V (Figure 3a, inset), we should examine the energy band diagram around the flat band condition and the contribution to the current due to thermionic emission and tunnelling of electrons. As shown in Figure 4c, electrons can accumulate at the InAs/InSe interface from which they can tunnel from the *n*-type InAs into the *p*-type InSe layers. At the flat band bias, $V = \phi_B$, electrons are injected from *n*-InAs to *p*-InSe through a potential barrier of height $\Delta E_C = 0.30$ eV. By increasing the bias to $V = \phi_B + \Delta E_C/e = 0.88$ V, the chemical potential in the *n*-type InAs aligns with the CB minimum of InSe, thus leading to a steeper increase of the current, as seen in the measured *I-V* at $V \sim 1$V (Figure 3a, inset). Similar "knees" in *I-V*s were reported in GaAs/(AlGa)As tunnel diodes and attributed to the formation of an accumulation layer

at the GaAs/(AlGa)As interface [22], a phenomenon analogous to that envisaged in our devices, and in hybrid *p*-*n* Ge/MoS_2 junctions [6], where they are attributed to tunneling.

We note that the band offset and bending of the InSe/InAs heterostructure is likely to be influenced by defect states at the interface [23]. Also, whereas surface states are not present in high concentration in InSe, they are known to exist in InAs, thus leading to the formation of a surface accumulation layer for electrons [24-25]. To examine its effect on the energy band profile of the InAs/InSe junction, we have solved the Poisson's equation for a junction containing a thin (1 nm) layer of ionized donors at the heterostructure interface with density of up to about 100 times the density of donors in the *n*-type InAs epilayer. We have found that this extra charge induces only a small change of the energy band profile. Thus, although we do not exclude the presence of defects at the InAs/InSe interface, our data and analysis suggest that these do not play a significant role in the rectification behavior observed in our devices.

The photoresponsivity of the junction is in line with the energy band diagram of Figure 4. Light creates photocarriers (electron-hole pairs) throughout the junction. In reverse bias (Figure 4d and $V < 0$), the photoelectrons are swept by the depletion field into the positively biased *n*-InAs, whereas the photogenerated holes move towards the negatively biased *p*-InSe. Because of the small dark current in reverse bias, the relative change of current due to the photogenerated carriers can be high. In particular, since the thickness of the depletion region W extends primarily into the *p*-InSe side of the junction ($W_p/W_n \sim 16$), the photocurrent is dominated by carriers photogenerated in InSe. Thus decreasing the photon energy from the band gap energy of InSe (E_g = 1.25 eV) towards that of InAs (E_g = 0.35 eV) causes a steep decrease of the photocurrent, as observed in the experiment at $V = 0$ and $V < 0$ (Figure 2).

In forward bias instead, the current arises from diffusion of majority carriers across the junction and the contribution of photogenerated carriers to the current should be generally smaller.

However, we observed a significant photoresponse around the "knee" in *I*-*V* at $V \sim 1$V. We explain this behaviour by considering the potential step ΔE_C at the heterojunction interface where the photogenerated electrons tend to accumulate on the *n*-side of the junction (Figure 4d and $V > 0$). Since this negative charge acts to screen the external electric field, under light illumination a larger applied voltage is needed to sustain the same current as in the dark. Thus under light illumination the "knee" in *I*-*V* shifts to higher biases and the current becomes smaller than that in the dark (Figure 3a, inset). Due to this electrostatic effect, the photocurrent is comparable to the dark current. Furthermore, this electrostatic effect disappears for sufficiently large biases as the photogenerated electrons acquire enough energy to cross the junction.

In summary, *n*-InAs/*p*-InSe heterojunctions exhibit diode-like behaviour and photoresponse in the visible and infrared spectral ranges with photoresponsivity of up to 0.2 A/W at λ=633 nm. The electrical properties can be explained by a type I band alignment for electrons and holes at the heterojunction interface. In our devices, the photoresponse originates primarily from light absorption in the *p*-InSe, which has a depletion width significantly wider than that for *n*-InAs. An InAs layer with a lower background concentration [26] comparable to that of *p*-InSe (10^{20} m^{-3}) and a small density of defect surface states may enable the fabrication of junctions with depletion regions equally distributed across both sides of the junction, thus leading to an improved photoresponse in the MIR range ($\lambda < 3.5$ μm).

Acknowledgements This work was supported by the EPSRC [under grants EP/M012700/1 and EP/J015296/1], the EU Graphene Flagship, the EU Marie Sklodowska-Curie ITN -PROMIS (641899), the University of Nottingham, and the Ukrainian Academy of Sciences.

References

[1] A. C. Ferrari, F. Bonaccorso, V. Fal'ko, K. S. Novoselov, S. Roche, P. Bøggild, S. Borini, F. H. L. Koppens, V. Palermo, N. Pugno, et al., Nanoscale **7**, 4598 (2015).

[2] S. Das, J. A. Robinson, M. Dubey, H. Terrones, and M. Terrones, Ann. Rev. Mater. Res. **45**, 1 (2015).

[3] Q. Zeng , H. Wang , W. Fu , Y. Gong , W. Zhou , P. M. Ajayan, J. Lou , and Z. Liu, Small **11**, 1868 (2015).

[4] S. Chuang, R. Kapadia, H. Fang, T. C Chang, W.-C. Yen, Yu-L. Chueh, and A. Javey, Appl. Phys. Lett. **102**, 242101 (2013).

[5] Y.J. Hong, J. W. Yang, W. H. Lee, R. S. Ruoff, K. S. Kim, and T. Fukui, Adv Mater. 25, 6847 (2013).

[6] D. Sarkar, X. Xie, W. Liu, W. Cao, J. Kang, Y. Gong, S. Kraemer, P. M. Ajayan, and K. Banerjee, Nature **526**, 91 (2015).

[7] A. Krier, Mid-infrared Semiconductor Optoelectronics, Springer Series in Optical Sciences, Vol. **118**, (2006).

[8] W. Feng, W. Zheng, W. Cao, and P. A. Hu, Adv. Mater. **26**, 6587 (2014).

[9] N. Balakrishnan, Z.R. Kudrynskyi, M.W. Fay, G.W. Mudd, S.A. Svatek, O. Makarovsky, Z. D. Kovalyuk, L. Eaves, P.H. Beton, and A. Patanè, Adv. Opt. Mater. **2**, 1064 (2014).

[10] G. W. Mudd, S. A Svatek, T. Ren, A. Patanè, O. Makarovsky, L. Eaves, P. H. Beton, Z. D. Kovalyuk, G. V Lashkarev, Z. R. Kudrynskyi, et al., Adv. Mater. **25**, 5714, (2013).

[11] A. Politano, G. Chiarello, R. Samnakay, G. Liu, B. Gürbulak, S. Duman, A. A. Balandinc, and D. W. Boukhvalovfg, Nanoscale **8**, 8474 (2016).

[12] G. W. Mudd, S. A. Svatek, L. Hague, O. Makarovsky, Z. R. Kudrynskyi, C. J. Mellor, P. H. Beton, L. Eaves, K. S. Novoselov, Z. D. Kovalyuk, et al., Adv. Mater. **27**, 3760 (2015).

[13] W. Feng, W. Zheng, X.S. Chen, G. Liu, W. Cao, and P.A. Hu, Chem. Mater. 27, 983 (2015)

[14] Z.R. Kudrynskyi, Z.D. Kovalyuk, V.M. Katerynchuk, V.V. Khomyak, I.G. Orletsky, and V.V. Netyaga, Acta Phys. Polonica A **124**, 720 (2013).

[15] Z. Kudrynskyi, V. Khomyak, V. Katerynchuk, M. Kovalyuka, V. Netyaga, and B. Kushnir, Thin Solid Films **582**, 253 (2015).

[16] S. Lei, X. Wang, B. Li, J. Kang, Y. He, A. George, L. Ge, Y. Gong, P. Dong, Z. Jin, et al., Nature Nanotechnology **11**, 465 (2016).

[17] Uli. Wurfel, D. Neher, A. Spies, and S. Albrecht, Nature Commun. **6**, 6951 (2015).

[18] F.J. Manjon, Y. van der Vijver, A. Segura and V. Munoz, Semicond. Sci. Technol. **15**, 806 (2000).

[19] A. Segura, J. Bouvier, M. V. Andres, F. J. Manjon, and V. Munoz, Phys. Rev. B **56**, 4075 (1997).

[20] The Fermi levels, $E_{F,}$ in the InSe and InAs layers are E_F = 0.30 eV above the valence band edge of InSe and E_F = 0.08 eV below the conduction band edge of InAs.

[21] S.M. Sze, Semiconductor Devices, Physics and Technology (2nd edition) John Wiley and Sons, Inc. 2002.

[22] E. T. Koenig, B. Jogai, M. J. Paulus, C. I. Huang, and C. A. Bozada, J. Appl. Phys. **68**, 3425 (1990).

[23] H.P. Hughes and H.I. Starnberg (eds.), Electron Spectroscopies Applied to Low-Dimensional Materials: Physics and Chemistry of Materials with Low-Dimensional Structures, Kluwer Academic Publisher 317-402 (Netherland 2002).

[24] W. Walukiewicz, Phys. Rev. B **37**, 4760 (1988).

[25] A. V. Velichko, A. Patanè, M. Capizzi, I. C. Sandall, D. Giubertoni, O. Makarovsky, A. Polimeni, A. Krier, Q.Zhuang, and C. H. Tan, Appl. Phys. Lett. **106**, 022111 (2015).

[26] A. R. J. Marshall, J. P. R. David, and C. H. Tan, IEEE Trans. Electron. Devices **57**, 2631 (2010).

FIGURE CAPTIONS

Figure 1. (a) Crystal structure of rhombohedral γ-InSe and zincblende InAs. **(b)** Current-voltage, *I-V*, characteristics for a series of *n*-InAs/*p*-InSe heterojunctions (T = 300 K) with in-plane area A = 2-5 mm^2. Inset: bias-dependence of the absolute current on a semi-logarithmic scale for two representative junctions.

Figure 2. Photocurrent spectra for two *n*-InAs/*p*-InSe heterojunctions at V=0 V and T=300 K. The insets show the calculated dependence of the periodicity ΔE of the interference pattern seen in the spectra on the thickness t of the *p*-InSe layer. As sketched in the inset, light propagates in the direction perpendicular to the layers of the heterojunction.

Figure 3. (a) Current-voltage, *I-V*, characteristics of an *n*-InAs/*p*-InSe heterojunction in the dark and under illumination with light of power P and wavelength λ = 984 nm (T = 300 K). Inset: *I-V*s at P = 0 (orange) and 6 μW (blue) revealing a steep increase of the current at $V \sim$ 1V. **(b)** Dependence of the photocurrent ΔI on V in reverse bias (P = 6 μW; λ = 984 nm). **(c)** Photoresponsivity R versus P at λ = 633 nm and 984 nm (V = 0 V).

Figure 4. Energy band diagrams for an *n*-InAs/*p*-InSe heterojunction at **(a)** V = 0 V, **(b)** $V < 0$ V, and **(c)** $V = \phi_B > 0$, where ϕ_B is the built-in potential at thermal equilibrium. The arrows show two transport processes: thermionic emission and tunnelling. **(d)** Sketches of the depletion region and of photogenerated carriers at $V < 0$ and $V > 0$. For $V > 0$ photogenerated electrons tend to accumulate at the heterojunction interface due to the potential step ΔE_C.

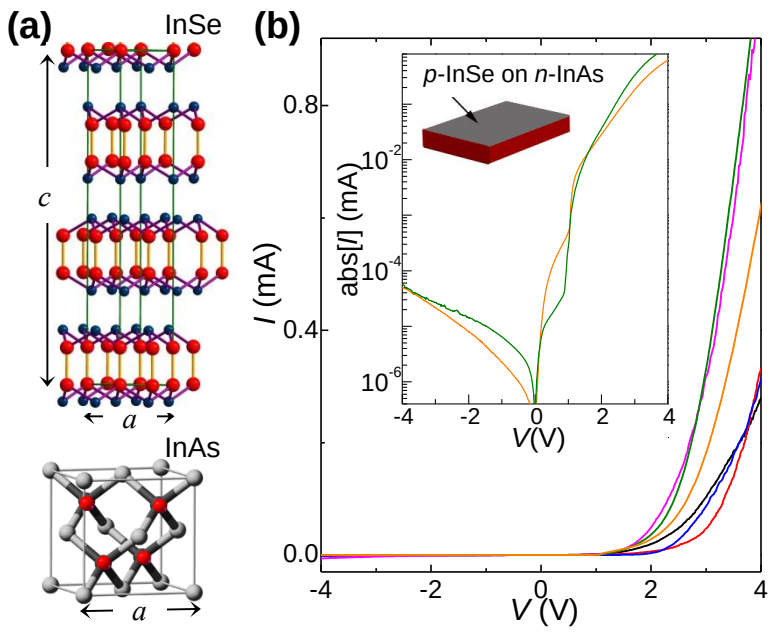
(a)
InSe
c
a
InAs
a
(b)
p-InSe on n-InAs
abs[I] (mA)
10-2
10-4
10-6
-4
-2
0
2
4
V(V)
I (mA)
0.8
0.4
0.0
-4
-2
0
2
4
V (V)

Figure 1

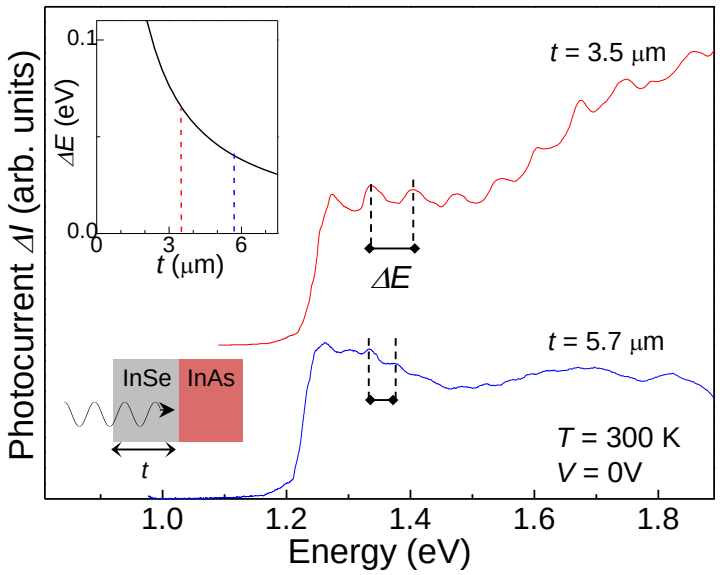
Photocurrent ΔI (arb. units)
Energy (eV)
1.0
1.2
1.4
1.6
1.8
t = 3.5 μm
t = 5.7 μm
ΔE
T = 300 K
V = 0V
InSe
InAs
t
ΔE (eV)
t (μm)
0.1
0.0
0
3
6

Figure 2

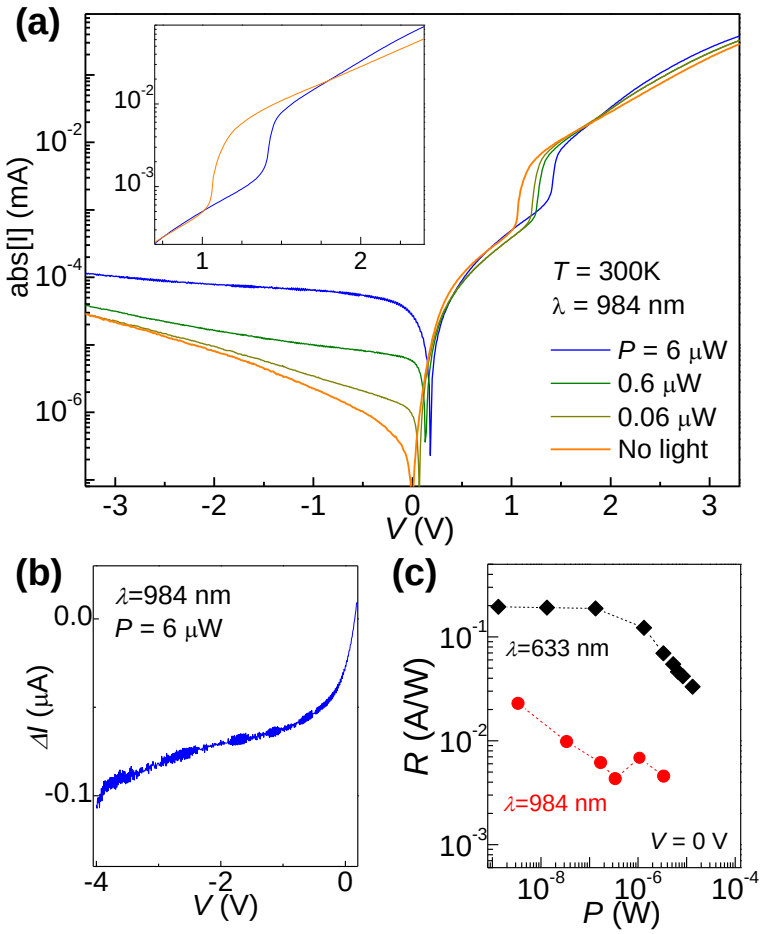
(a)
abs[I] (mA)
V (V)
T = 300K
λ = 984 nm
P = 6 μW
0.6 μW
0.06 μW
No light
(b)
λ=984 nm
P = 6 μW
ΔI (μA)
V (V)
(c)
λ=633 nm
λ=984 nm
V = 0 V
R (A/W)
P (W)

Figure 3

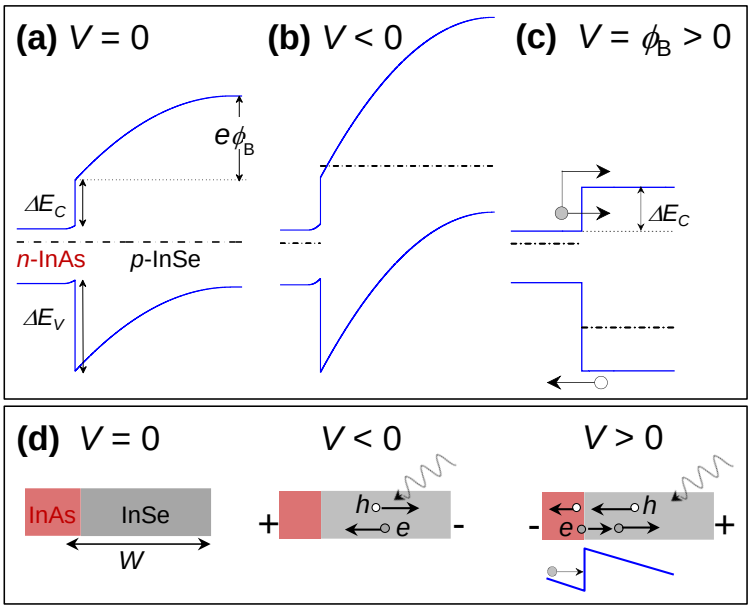
(a) V = 0
(b) V < 0
(c) V = ϕB > 0
eϕB
ΔEC
n-InAs
p-InSe
ΔEV
ΔEC
(d) V = 0
V < 0
V > 0
InAs
InSe
W
+
h
e
-
-
e
h
+

Figure 4